ACS APPLIED MATERIALS & INTERFACES

Research Article

www.acsami.org

Interface Behaviors of Acetylene and Ethylene Molecules with 1-Butyl-3-methylimidazolium Acetate Ionic Liquid: A Combined Quantum Chemistry Calculation and Molecular Dynamics Simulation Study

Hao Xu,[†] Zhe Han,[‡] Dongju Zhang,[†,*] and Jinhua Zhan[†]

[†]Key Laboratory of Colloid and Interface Chemistry, Ministry of Education; School of Chemistry and Chemical Engineering, Shandong University, Jinan, 250100, P. R. China

[‡]New Materials Institute of Shandong Academy of Sciences, Jinan, 250014, P. R. China

ABSTRACT: Although imidazolium-based ionic liquids (ILs) combined with oxygen-containing anions were proposed as the potential solvents for the selective separation of acetylene (C_2H_2) and ethylene (C_2H_4), the detailed mechanism at the molecular level is still not well understood. The present work focuses on a most effective IL for removing C_2H_2 from a C_2H_4 stream, 1-butyl-3-methylimidazolium acetate ([BMIM][OAc]), aiming at understanding the first steps of the adsorption process of the molecules at the IL surface. We present a combined quantum mechanical (QM) calculation and molecular dynamics (MD) simulation study on the structure and property of the IL as well as its interaction with C_2H_2 and C_2H_4 molecules. The calculated results indicate that C_2H_2 presents a stronger interaction with the IL than C_2H_4 and the anion of the IL is mainly responsible for the stronger interaction. QM calculations show a stronger hydrogen-binding linkage between an acidic proton of C_2H_2/C_2H_4 and the basic oxygen atom in $[OAc]^-$ anion, in contrast to the relative weaker association via the C−H···π interaction between C_2H_2/C_2H_4 and the cation. From MD simulations, it is observed that in the interfacial region, the butyl chain of cations and methyl of anions point into the vapor phase. The coming molecules on the IL surface may be initially wrapped by the extensive butyl chain and then devolved to the interface or caught into the bulk by the anion of IL. The introduction of guest molecules significantly influences the anion distribution and orientation on the interface, but the cations are not disturbed because of their larger volume and relatively weaker interaction with the changes in the guest molecules. The theoretical results provide insight into the molecular mechanism of the observed selective separation of C_2H_2 form a C_2H_4 stream by ILs.

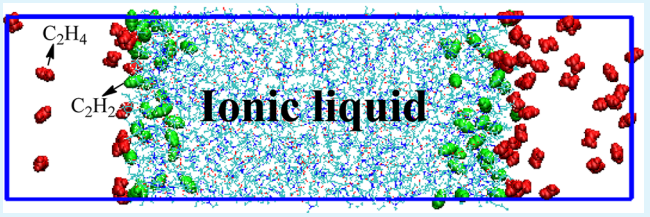

KEYWORDS: *acetylene, ethylene, ionic liquids, 1-butyl-3-methylimidazolium acetate, quantum chemistry, molecular dynamics*

1. INTRODUCTION

Ethylene (C_2H_4), the simplest alkene, is one of the most important raw materials for many industrial products such as plastics, rubbers, alcohols. It is normally produced from the thermal or catalytic cracking process of petroleum or natural gas.[1,2] Usually, in the product of ethylene there is a small amount of acetylene (C_2H_2) impurities that can cause catalyst poisoning in the ethylene polymerization process and also lower the quality of polymerized product.[3] Moreover, acetylene may convert into solid thus blocking fluid stream and even resulting in explosion.[4] So it is essential to remove acetylene impurities from ethylene for a wide range of manufacturing processes of petrochemical products, particularly polyethylene plastics. However, the separation of acetylene from an ethylene stream is complex and costly because of the close boiling points of these two unsaturated hydrocarbons.[2] At present, there are two major methods used for the purification of ethylene: catalytic hydrogenation of acetylene over noble metal catalysts like Pd[3,4] and solvent extraction using organic solvents (e.g., *N*,*N*-dimethylformamide or *N*-methylpyrrolidinone).[5] There exist many disadvantages of these traditional processes. For example, the former can cause overhydrogenation of ethylene into ethane, while the letter can result in the loss of organic solvents.[6]

Ionic liquids (ILs) are generally composed of large organic cations (such as alkylimidazolium, alkylpyridimium, and tetraalkylammonium) and small inorganic anions (such as Cl^-, NO_3^-, BF_4^-, and PF_6^-),[7−9] and their melting point generally less than 100 °C. In the past decades, ILs have been attracted more and more attention[10−13] because of their many remarkable physicochemical properties,[14−17] such as high thermal and chemical stability, negligible vapor pressure, wide liquid range, reusablility, and designability, which make ILs widely used in chemical synthesis and extraction separation processes, and a considerable amount of literature has been published on the application of ILs.[18−21]

Received: August 27, 2012
Accepted: December 4, 2012
Published: December 4, 2012

Recently, Palgunadi and Kim et al.[6,22−24] reported the highly efficient selective removal of C_2H_2 from a C_2H_4 stream by imidazolium-based ILs combined with various oxygen-containing anions such as dialkylphosphate ($[Me_2PO_4]^-$), methylphosphonate ($[MeHPO_3]^-$), or acetate ($[OAc]^-$). Through the ^1H NMR experiments[6,23] they conjectured that this phenomenon is due to the stronger interaction of acetylene with the IL than that of ethylene. Moreover by performing quantum mechanics-based calculations[23] they showed that the acidic proton of acetylene forms strong hydrogen bond with the basic oxygen atom of the anion, whereas the acidic protons on the cation do not specifically associate with the π cloud of acetylene. Very recently, to understand the differential solubility of C_2H_2 and C_2H_4 in ILs, Xing et al.[25] presented a detailed theoretical study of the interaction mechanisms between C_2H_2/C_2H_4 and three typical ILs, [BMIM][BF_4], [BMIM][Tf_2N], and [BMIM][OAc]. Based on the results of the natural bond orbital (NBO) analysis and the atoms in molecules (AIM) analysis, they proposed that the hydrogen-bonding interaction in the C_2H_2-anion is mainly responsible for the large solubility of C_2H_2 in the ILs, whereas such a interaction is much weaker in C_2H_4-anion and comparable with the $p-\pi$ interaction in the C_2H_4-anion complexes and the $\pi-\pi$ interaction in the C_2H_4-cation complexes. These existing studies provide valuable guidance to understand the differential solubility of C_2H_4 and C_2H_2 in the ILs.

As far as we know, however, little attention has been paid to the interfacial structure and property between an IL and $C_2H_4-C_2H_2$ gas, which is of intrinsic importance for understanding the separation behavior of $C_2H_4-C_2H_2$ gas by the ILs. To address this issue, we here present a combined quantum mechanics-based (QM) calculation and molecular dynamics (MD) simulation study, where 1-butyl-3-methylimidazolium acetate ([BMIM][OAc]), one of the most efficient C_2H_2/C_2H_4 separation mediums, is chosen as a representative of the imidazolium-based ILs separating C_2H_4 and C_2H_2 used in the experiments.[6,22−24] The outline of this article is organized as follows: Section 2 describes the computational methodology and procedure employed in this study. Results and discussion are given in Section 3, and conclusions are outlined in Section 4.

2. COMPUTATIONAL DETAILS

QM calculations were carried out for the isolated cation $[BMIM]^+$, anion $[OAc]^-$, and ion pair [BMIM][OAc], as well as their respective complexes with C_2H_2 and C_2H_4 molecules, within the framework of density functional theory (DFT) using the B3LYP functional with the standard 6-31++G(d,p) basis set, as implemented in Gaussian 03 program package.[26] Vibrational frequencies were also calculated at the same level of theory to check whether the optimized structures correspond to a true local minima or not and to provide zero-point vibrational energies (ZPEs). The optimized structures were then used as basic structural units to build the models for the following MD simulations.

AMBER force field[27] was employed in our MD study. For the $[BMIM]^+$ cation, we used the force field parameters developed by Wang et al.[28] However, AMBER force field has not special parameters for the anion $[OAc]^-$ as well as C_2H_2 and C_2H_4 molecules. In the present simulation, these force-field parameters were borrowed from the generalized AMBER force field (GAFF),[29] and the atomic charge assignments were calculated by fitting the electrostatic potential (ESP)[30,31] of optimized structures using the Moller−Plesset second-order perturbation theory (MP2)[32,33] and the 6-31++G(d,p) basis set. Our preliminary simulation shows that the liquid density (1.066 g cm^{-3}) obtained using the ESP charges is in better agreement with the experiment (1.055 g cm^{-3}) than that (1.074 g cm^{-3}) obtained using the GAFF charges. In addition, such a combined force field parameter method has been also proposed in the recent publications of IL simulations.[34,35] So the present simulations used the ESP charges instead of the GAFF charges.

The GROMACS 4.5.1[36−39] software package was used for all MD simulations in this study. Leapfrog algorithm was used to integrate the Newton's equations of motion. The time step was set to 1 fs, and data were collected every 1000 time steps for analysis. The long-range electrostatic interactions were computed by using the particle mesh Ewald method,[40,41] with a cutoff distance of 1.2 nm. Edge and finite size effects are minimized by applying periodic boundary condition, and a switching function was used to smoothly truncate the van der Waals potential at the cutoff distance.

MD simulations were performed for the following three systems: (1) the pure IL system, (2) IL−vacuum interface system, and (3) IL−gas interface system. The pure IL system containing 250 [BMIM]-[OAc] ion pairs was first energetically minimized using the steepest descent method, then equilibrated in the NVT ensemble for 3 ns. Because the equilibrium state of a system can be reached easily at high temperatures, the simulations in the NPT ensemble (P = 1 bar) were first carried out at 600 K for 5 ns and then cooled down to the target temperature 298 K to obtain the liquid density for comparison with the experimental value. Finally, an additional 5 ns production simulation was performed at 298 k in the NPT ensemble, from which data were collected for analysis. For the liquid-vacuum system, we doubled the size of the pure IL system in the z-direction and then extend 60 Å along z-axis leading to create a ∼43 × 43 × 146 Å simulation box containing 500 [BMIM][OAc] ion pairs, where the height of two vacuum phases are 30 Å. The system was then equilibrated at 313 K for 5 ns in the NVT ensemble. Following this, another 5 ns simulation was carried out to create two liquid−vacuum interfaces that were parallel to the xy-plane. After that, we randomly placed 25 C_2H_2 and 25 C_2H_2 molecules in the vacuum region to build the initial liquid−gas interface system, from which we carried out the MD simulation in the NVT ensemble for 20 ns. The target temperature was set at 313 K, the temperature used in the experiments.[6,22−24] The Berendsen thermostat and barostat algorithm[42] were utilized in all MD simulations.

3. RESULTS AND DISCUSSION

3.1. Quantum Chemistry Calculations. Figure 1 shows the optimized geometries of cation $[BMIM]^+$, anion $[OAc]^-$, and ion pair $[BMIM]^+[OAc]^-$ by performing QM calculations. It is found that the ion pair is the most stable as the $[OAc]^-$ anion occurs in the vicinity of the C2−H bond of the cation as given in Figure 1c. This can be attributed to the larger positive charge on the C2−H units (0.176 e), than on other C−H units. In $[BMIM]^+[OAc]^-$ there exist two C−H···O hydrogen bonds, as shown by the calculated the small H···O distances (1.629 and 2.033 Å, which are shorter than the summation of the van der Waals radii of O and H, 2.72 Å)[43] and the quasi-linear C−H···O angles (165.2 and 169.3°). The energy of formation of the ion pair is calculated to be 98.15 kcal mol^{-1}. The effective hydrogen bond and the strong Coulomb interaction between the cation and anion are in agreement with the observed physicochemical properties of [BMIM][OAc] ionic liquid, for example, high viscosity, low vapor pressure, and good thermal stability.

The calculated complex structures of the cation, anion, and ion pair with C_2H_2/C_2H_4 are also shown in Figure 1. In the complexes of the ion pair with C_2H_2/C_2H_4, it is found that both C_2H_2 and C_2H_4 mainly interact with the anion through their C−H units to form new C−H···O hydrogen bonds (1.934 Å in the former and 2.280 Å in the latter), which weaken the C−H···O hydrogen bonds in the ion pair. The calculated interaction energies of C_2H_2 and C_2H_4 with the ion pair are

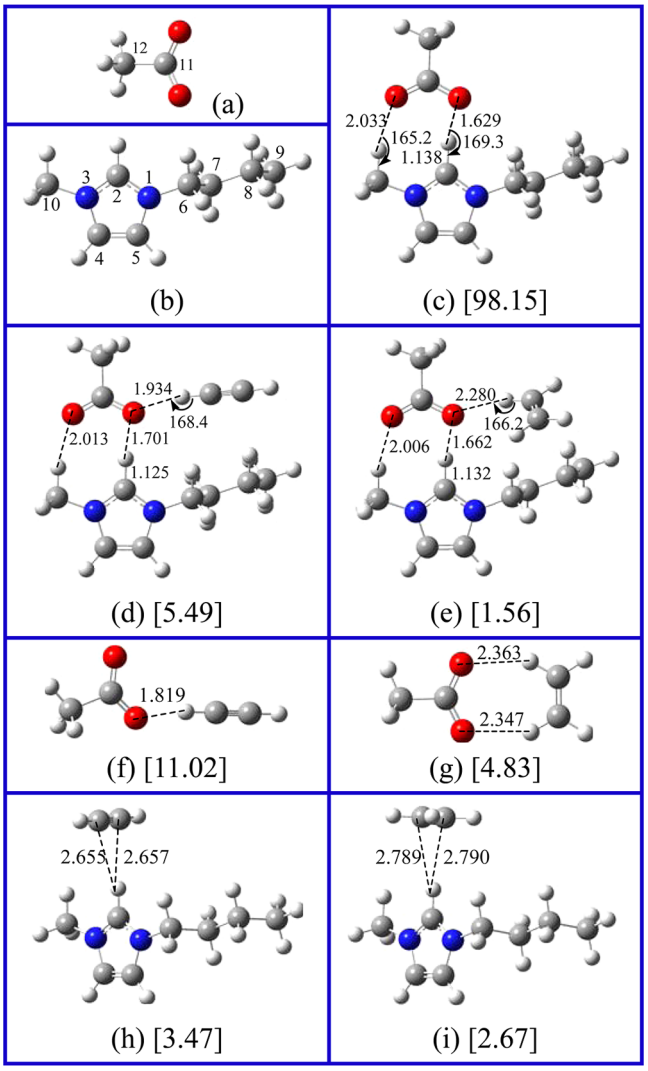

Figure 1. Optimized geometries at the B3LYP/6-31++G(d,p) level for (a) the isolated single anion, (b) cation, (c) ion pair, the complexes of (d, f, h) acetylene and (e, g, i) ethylene with the ion pair, anion, and cation. Atomic numbers are given in panels a and b. Bond distances are shown in Angstrom, and the angles are in degree. The values in square brackets are the calculated interaction energies (in kcal/mol).

5.49 and 1.56 kcal mol^{-1}, respectively. From these data, it is clear that C_2H_2 presents a stronger hydrogen-bonding-type interaction with the ion pair than C_2H_4.

As observing the anion-molecule and cation-molecule complexes, we find that the former is more favorable in energy than the latter. In the former, C_2H_2 and C_2H_4 associate to the anion via hydrogen bonds, while in the later, they attach to the cation through C−H···π interactions. Furthermore, it is also very clear that C_2H_2 presents stronger capacity to form both the anion- and cation-cmplexes than C_2H_4. According to these results, we can basically understand the observed selective removal of C_2H_2 from a C_2H_4 stream by the IL.[6,22−24] We believe that the IL anion plays a crucial role in this separation process.

3.2. MD Simulation on Pure [BMIM][OAc]. As described in the computational details, we carried out a 5 ns MD production run on the [BMIM][OAc] system containing 250 ion pairs. From the equilibrated system, the liquid density is found to be 1.066 g cm^{-3}, which is within 1% of the experimental value of 1.055 g cm^{-3}.[44] According to the Stokes−Einstein relation,[45] the estimated viscosity of the IL from the self-diffusion coefficients of the cations and anions (1.81×10^{-12} and 2.06×10^{-12} m^2 s^{-1}) is about 1.07 Pa s. This value is higher than that of water (0.9 mPa s),[46] which is consistent with the previous literature.[45]

To analyze the local structure of the IL, we calculated the radial distribution functions (RDFs) and spatial distribution functions (SDFs). In Figure 2a, all three RDFs show strong and damped oscillations within 2 nm which coincide with the feature of a strongly coupled ionic system.[47] The first peak of $g(r)_{ca}$ locating at about 0.5 nm, is much stronger than those of

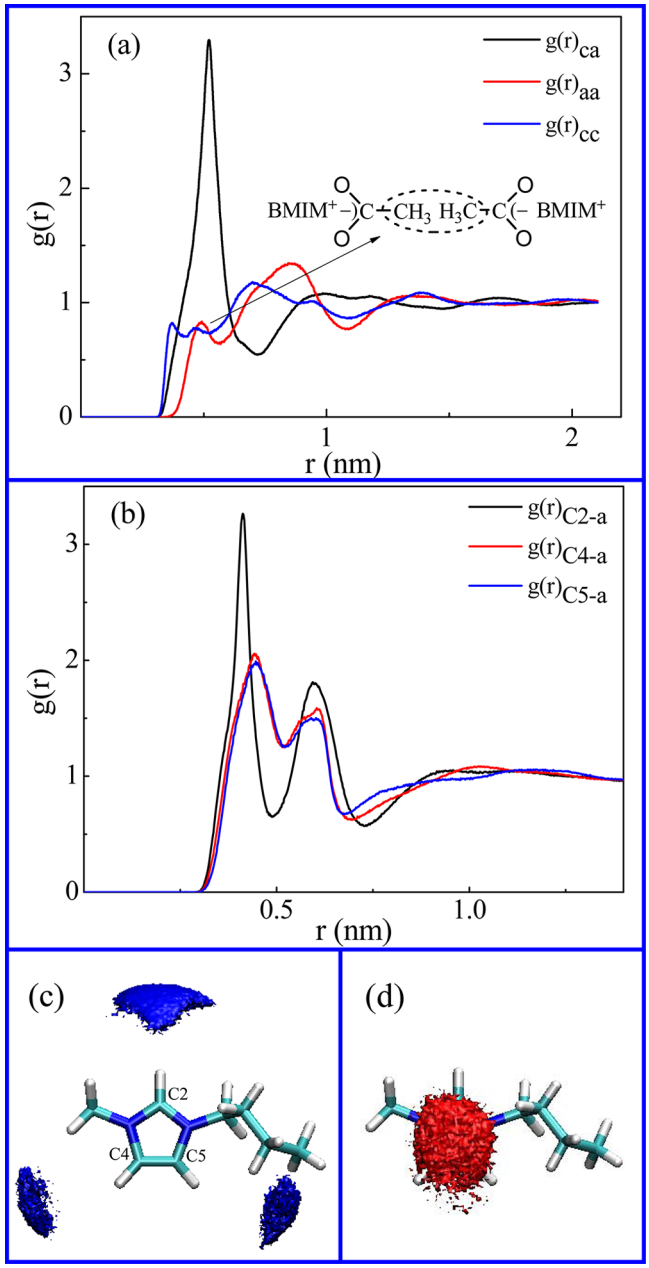

Figure 2. (a) RDFs of the cation−anion, anion−anion, and cation−cation pairs, where the inset shows schematic drawing for the formation of anion methyl−methyl contacts. (b) RDFs for the selected atom-anion pairs. (c) Colored SDFs within 0.7 nm for anions around a cation (isosurface value: 0.032 Å^{-3}). (d) Colored SDFs within 0.7 nm for cations around a cation (isosurface value: 0.018 Å^{-3}).

dx.doi.org/10.1021/am301796w | ACS Appl. Mater. Interfaces 2012, 4, 6646−6653

$g(r)_{cc}$ and $g(r)_{aa}$ due to the strong cations-anions electrostatic attraction. The $g(r)_{aa}$ and $g(r)_{cc}$ show shoulders around 0.5 and 0.4 nm, which are believed to originate from the anion methyl−methyl contacts[48] and the cation $\pi-\pi$ stacking,[49] respectively. The calculated distance between inidazolium rings (0.37 nm) provide support for the claim of the $\pi-\pi$ stacking. Furthermore, the maxima of $g(r)_{ca}$ coincide with the minima of $g(r)_{cc}$ and $g(r)_{aa}$ with just a little shifts and vice versa. This feature shows a long-range ordered structure of [BMIM][OAc]. Figure 2b shows the RDFs of several selected atom-anion pairs, including C2-, C4-, and C5-anion airs. Three major peaks at about 0.4−0.45 nm indicate the strong interaction of anion with the cation at these sites. However, the amplitude of these three RDFs is different: $g(r)_{C2\text{-}a}$ has the strongest peak and is located at the smallest distance, indicating the anions prefer to occur at the vicinity of C2 site of the cations. This is in line with the result of QM calculations above (see panel c in Figure 1). Panels c and d in Figure 2 show calculated three-dimensional structures of SDFs within 0.7 nm of anions or cations around a cation. Three large lobes in Figure 2c, directing roughly along the C2−H, C4−H, and C5−H bonds, indicate that the anions lie mainly in the vicinity of these bonds, i.e., the anions are highly directed. From Figure 2d, we find that the cations mainly occur in the areas above and below the imidazolium ring locating about 0.35 nm from the cation center via the $\pi-\pi$ stacking of the imidazolium rings, which accounts for the shoulder around 0.4 nm in $g(r)_{cc}$ in Figure 2a.

3.3. MD Simulation on IL−Vacuum System. It is well-known that properties and concentrations of a liquid at its interface are generally very different from its bulk,[50] and so also are for ILs. Many applications of ILs are related to their interfacial characteristic and structures, especially for multiphasic catalysis. Many experimental[51−53] and computational[54−56] studies have been performed to understand the interfacial properties of ILs. For the gas-sorption behavior concerned in this work, the interfacial property of ILs even play a critical role because any gas molecule that is solvated would first come to the surface of ILs and then crosses into the bulk phase. Here we present the liquid−vacuum interfacial properties of [BMIM][OAc].

We first calculated the surface tension of IL−vacuum system form the difference between the normal and the lateral pressure. The average value of the surface tension is about 38.3 mN m^{-1}, which falls inside the range of the experimental data (~30−50 mN m^{-1}) for imidazolium-based ILs. In Figure 3a, we show the mass density profile of the IL−vacuum system along the z-axis. It is found that the mass density distribution shows an oscillation throughout the whole liquid phase and that there is a significant enhancement of density at the interface region. This indicates that the liquid density is not uniform even in the bulk phase and that at the surface there exists a dense region, in which the liquid density is larger than its bulk density.

Figure 3b presents the number density profiles of anion and cation centers. For the cation, the center is defined to be the ring center, while the center of mass is used for the anion. Pronounced oscillations are observed for both the ions, and there is some reverse correlation between the anion and cation number densities, implying that there is a fair structural ordering (layering) throughout the whole liquid. The number density of cations is significantly enhanced near the interfacial region, and that of anions is slightly enhanced inner the interfacial region by ~3 Å, indicating that the cation is mainly

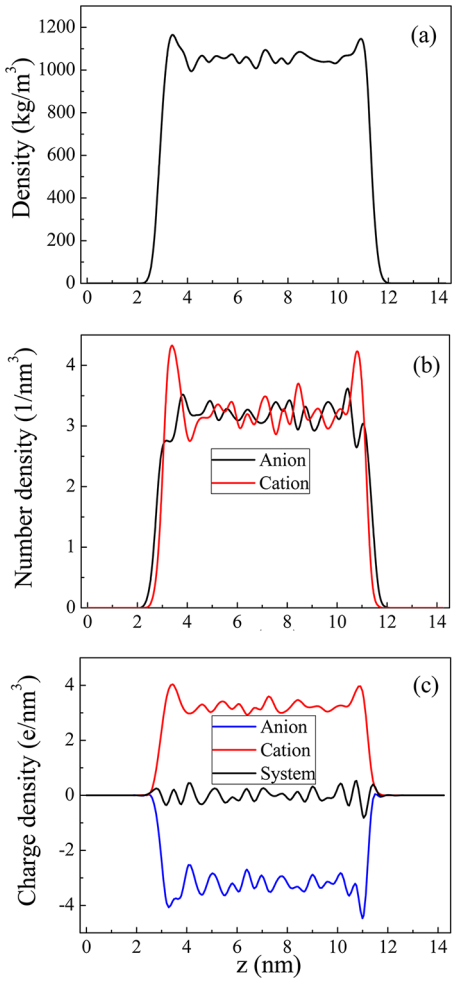

Figure 3. (a) Mass density profile for the [BMIM][OAc] system along the z-axis. (b) Number density profiles of anion and cation. The imidazolium ring and the entire acetate molecule were taken as the center of the cation and anion. (c) Charge density profiles of anion, cation, and system.

responsible for the enhanced density near the interface region in Figure 3a.

Figure 3c shows the charge density profiles of anions and cations, as well as their sum (the total charge density). Both the cation and anion show oscillations and have a maximum near the interface, which is consistent with the mass and number density profiles shown in panels a and b in Figure 3. The total charge density profile fluctuates around zero, showing the liquid system is essentially neutral throughout the whole depth profile.

Panels a and b in Figure 4 show the number density profiles for some selected atoms in the cation and the anion. As shown in Figure 4a, the peak positions of profiles for several atoms in the cation are in the order of C9 > C8 > C7 > C6 > N1 > N3 > C10, indicating that the butyl chain orients along the normal of interface and points into the vacuum. In Figure 3b, the order of peak positions for the selected atoms in anion is H > C12 > C11 > O, which demonstrates that the methyl of acetate anions points into the vacuum and the carboxyl orients inside of the interface. Figure 4c gives a diagrammatic sketch describing the orientation of the cations and anions at the interface. The features of the liquid−vacuum interface of [BMIM][OAc] we found are in common with some other ILs.[57,58]

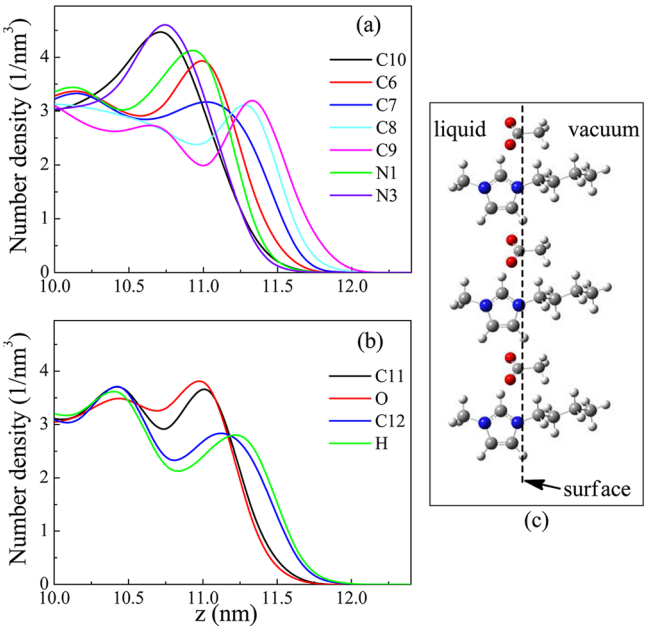

Figure 4. Number density profiles for individual atoms of cation (a) and anion (b) at the interface region of the IL–vacuum system. (c) Diagram showing the orientation of the cations and anions at the interface.

3.4. MD Simulation on IL–Gas Interface. In this section, we show the results of MD simulations on the interfacial system composed of the IL and gas molecules (C_2H_2 and C_2H_4). Panels b and c in Figure 5 show the initial and final snapshots of the IL–gas system, where the IL–vacuum system at equilibrium (Figure 5a) is also given for comparison. In Figure 5b, C_2H_2 and C_2H_4 molecules were initially randomly distributed in the cell, where molecules are dyed by two different colors (C_2H_2: green, C_2H_4: red) for easy distinction. After the MD simulation, as shown in Figure 5c, almost all

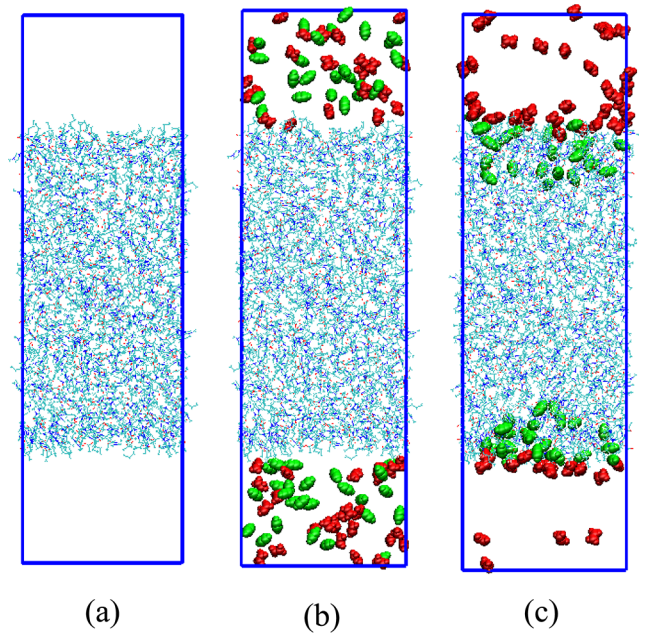

Figure 5. (a) IL–vacuum system, (b) initial, and (c) final of IL–gas system snapshots. Color code: acetylene, green; ethylene, red.

C_2H_2 molecules cross the interface to migrate into the IL bulk phase, which is in contrast to the behavior of C_2H_4 molecules that some of them still stay in gas phase although the molecules near the interface have a large proportion.

Figure 6 shows the calculated number density profiles of anions and cations, as well as C_2H_2 and C_2H_4 molecules.

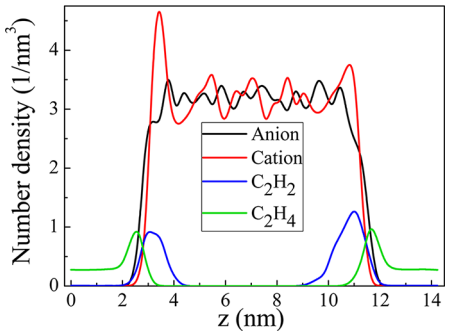

Figure 6. Number density profiles of the IL–gas interfacial system along the *z*-axis (black, red, blue, green lines are for anions, cation, C_2H_2, and C_2H_4, respectively).

Compared to the IL–vacuum system, it is found that the interfaces of IL–gas system are slightly expanded along both the directions. We also note that at the interface region the number densities of both the cation and anion are remarkably changed upon the presence of C_2H_2 and C_2H_4 molecules. For the anion, its number density at the interfacial region is now not obviously different from its bulk value, although that of the cation still presents a pronounced enhancement at the interface region as in the IL–vacuum system. This indicates that the guest molecules show more a stronger interaction with anions than with cations. For both C_2H_2 and C_2H_4 molecules, the maximum peaks are observed near the interface region. As displayed in Figure 6, the C_2H_2 peaks (blue lines) are higher than those of C_2H_4 (green lines). And further the former almost enters the bulk, whereas the latter occurs at the interface. These results are consistent with the snapshots shown in Figure 5c.

To further understand the dynamic process of C_2H_2 and C_2H_4 at the interface region, we calculated the number density profiles of C_2H_2 and C_2H_4 molecules at four different time points during the 20 ns simulation at one side interface of the IL–gas system, as shown in Figure 7, where the number density profiles of the cation and anion are also reproduced for easy assignation for the interface. At 0 ns, the peaks of the number density profiles for both C_2H_2 and C_2H_4 molecules are broader and unapparent at the interface regions, because the gas molecules were initially scattered randomly in the cell. For C_2H_2 molecules (Figure 7a), when the simulation was carried out for 0.5 ns, an obvious number density peak can be seen in the interfacial region, indicating that a C_2H_2 adsorption layer has been formed at the interface. With the simulation time increases, the C_2H_2 peak gradually moves into the bulk, and when the simulation is carried out for 20 ns all C_2H_2 molecules either enter into the bulk or stay at the interfacial region. In contrast, for C_2H_4 molecules (Figure 7b), throughout all time points, the number density profiles present maximum only at the interfacial region and a remarkable number of C_2H_2 is found to occur in the gas-phase region. These results show the dynamic process of C_2H_2 and C_2H_4 molecules diffusion into

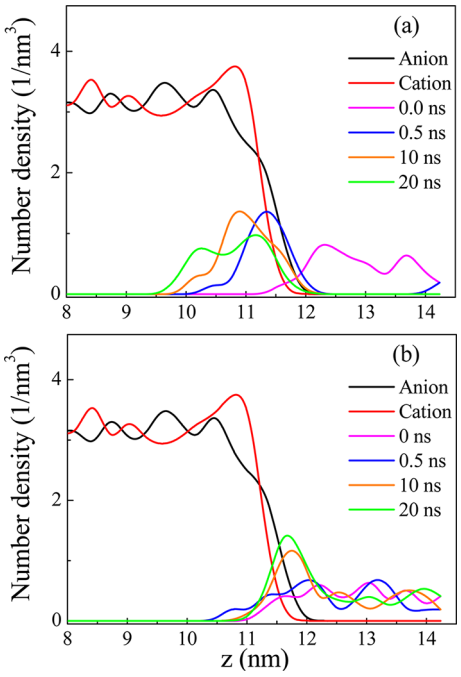

Figure 7. Evolution of number density at four different time points for (a) C_2H_2 and (b) C_2H_4 at the interface region of the IL–gas system.

the IL. The formation of the adsorption layer of C_2H_2 at the IL surface is much faster on the interface than that of C_2H_4.

Figure 8 gives the calculated number density profiles of selected atoms in the cations and anions at the interface region

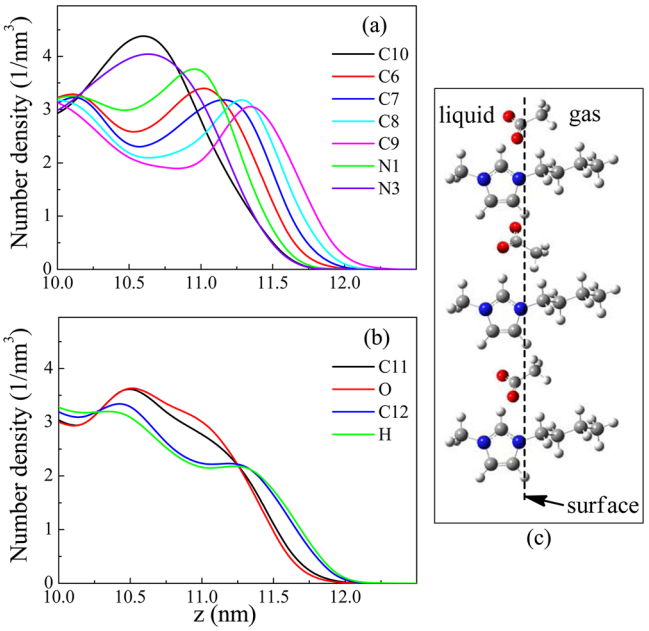

Figure 8. Number density profiles for individual atoms of cation (a) and anion (b) at the interface region of the IL–gas system. (c) Diagram showing the inferred orientation of the cations and anions.

of the IL–gas system. We note that the interface region of the IL–gas system is slightly expanded along *z*-axis, and it occurs at about 12.3 nm in the *z*-direction, which is in contrast with the IL–vacuum system with an interface at about 12.0 nm. This phenomenon coincides with the interface expansion shown in Figure 6. In Figure 8a, we find that the peak positions of the C6 and successive C7, C8, and C9 atoms on the butyl group locate progressively along *z*-direction, indicating that the butyl chain points into the gas phase, which is similar with the distribution of the cations in IL–vacuum system. In addition, the number density profiles and heights of the selected atoms in the cation are also similar to those shown in Figure 4a. In contrast, from Figure 8b, we found that the number density profiles of the selected atoms in the anion is distinctly different from those in the IL–vacuum system, and their height are obviously lower than the corresponding those shown in Figure 4b. These data indicate that upon the adsorption/absorption of C_2H_2 and C_2H_4, the distribution of the cations near the interface is not almost affected, while the anions orientation has a significant change. This can be attributed to the larger volume of the cation and its weaker interaction with the guest molecules in comparison with the anion. Figure 8c shows a diagrammatic sketch describing the orientation of the cations and anions at the interface upon the adsorption/absorption of C_2H_2 and C_2H_4.

Furthermore, we calculated the interaction energies (ΔE) between C_2H_2/C_2H_4 and $[BMIM]^+/[OAc]^-$. ΔE is defined as the summation of electrostatic energy (ΔE_{Coul}) and van der Waals interaction energy (ΔE_{LJ}) using eq 1:[59,60]

$$\Delta E = \Delta E_{Coul} + \Delta E_{LJ} \quad (1)$$

Table 1 lists the calculated mean contributions of Coulomb and Lennard-Jones interactions to ΔE. It is found that the Coulomb

Table 1. Mean Values of Coulomb and Lennard–Jones Interaction Energies (in kJ mol^{-1}) between C_2H_2/C_2H_4 and $[BMIM]^+/[OAc]^-$

	ΔE_{Coul}	ΔE_{LJ}	ΔE
$[OAc]^-$–C_2H_2	−33.13	−4.38	−37.51
$[BMIM]^+$–C_2H_2	5.41	−22.92	−17.51
$[OAc]^-$–C_2H_4	−1.34	−0.99	−2.33
$[BMIM]^+$–C_2H_4	0.87	−2.93	−2.06

attraction is dominant in $[OAc]^-$–C_2H_2 interaction, although the van der Waals attraction is primary in $[BMIM]^+$–C_2H_2 interaction. In contrast, although the Coulomb attraction is comparable with the van der Waals force in $[OAc]^-$–C_2H_4 interaction, the van der Waals attraction is slightly stronger than the Coulomb repulsion in $[BMIM]^+$–C_2H_4. Furthermore, the mean value of $[OAc]^-$–C_2H_2 interaction energy is −37.51 kJ mol^{-1}, which are twice greater in absolute value than $[BMIM]^+$-C_2H_2 interaction energy (−17.51 kJ mol^{-1}). These two interaction energies are much larger in absolute value the corresponding those for $[OAc]^-$–C_2H_4 and $[BMIM]^+$–C_2H_4 interactions (−2.33 and −2.06 kJ mol^{-1}). These results suggest again that the anions play a much more important role than the cations for the absorption of acetylene in the IL, and that the strong Coulomb interaction between anions and acetylene is the major factor in the separation process of C_2H_2 using [BMIM][OAc].

On the basis of the results of MD simulations above, we can envisage the selective separation process of C_2H_2 and C_2H_4 by [BMIM][OAc] as follow: C_2H_2 and C_2H_4 molecules are initially wrapped by the cation butyl chain oriented along the normal of interface, then devolved to the interface. C_2H_2 molecules bound on the interface can further dragged into the bulk by the IL anion, whereas most of C_2H_4 molecules gather at the interface region and reach dynamic adsorption/

dx.doi.org/10.1021/am301796w | ACS Appl. Mater. Interfaces 2012, 4, 6646–6653

desorption balance on the interface. This scene is diagrammatically shown in Figure 9.

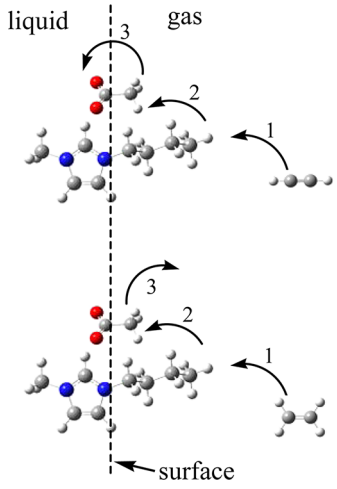

Figure 9. Diagram showing the selective separation process of C_2H_2 and C_2H_4 by [BMIM][OAc].

4. CONCLUSIONS

In summary, we have carried out a combined QM calculation and MD simulation study to better understand the removal mechanism of C_2H_2 from a C_2H_4 stream by [BMIM][OAc]. Based on the calculated interaction energies, it is proposed that both C_2H_2 and C_2H_4 molecules prefer to link to the anion of IL via the hydrogen bonding interaction between an acidic proton of C_2H_2/C_2H_4 and the basic oxygen atom in $[OAc]^-$ and link to the cation of IL via the C−H···π interaction between the C−H bond of C_2H_2/C_2H_4 and the imidazolium ring of the cation. However, the interaction of C_2H_2 with the cation, anion, and ion pair are found to be stronger than those of C_2H_4. The different interaction results in the selective separation of C_2H_2 and C_2H_4 by the IL. MD simulations show that in the interfacial region the butyl chain of cations and the methyl of anions point into the vapor phase. Upon the adsorption/absorption of C_2H_2 and C_2H_4, the distribution of the cations near the interface is almost not affected, while the anions orientation has a significant change. On the basis of the theoretical results, a clear picture of the C_2H_2 removal from a C_2H_4 stream can be imagined as follows: the cation butyl chain of the IL initially wraps C_2H_2 and C_2H_4 molecules and further devolves them to the interface, C_2H_2 molecules bound on the interface are further dragged into the bulk by the IL anion, whereas most of the C_2H_4 molecules stick to the surface. The present results provide guidance for understanding the observed selective separation of C_2H_2 form a C_2H_4 stream by ILs.

AUTHOR INFORMATION

Corresponding Author

*E-mail: zhangdj@sdu.edu.cn. Phone: +86-531-88365833. Fax: +86-531-88564464.

Notes

The authors declare no competing financial interest.

ACKNOWLEDGMENTS

This work was jointly supported by National Basic Research Program of China (973 Program, 2013CB934301), National Natural Science Foundation of China (NSFC 21273131), and the Graduate Independent Innovation Foundation of Shandong University (yzc12108).

REFERENCES

(1) Pässler, P.; Hefner, W.; Buckl, K.; Meinass, H.; Meiswinkel., A.; Wernicke, H.; Ebersberg, G.; Müller, R.; Bässler, J.; Behringer, H.; Mayer, D. *Ullmann's Encyclopedia of Industrial Chemistry*; Wiley-VCH: Weinheim, Germany, 2007.
(2) Roberts, L. R. *Encyclopedia of Chemical Processing and Design* **1976**, *1*, 363−382.
(3) Huang, W.; McCormick, J. R.; Lobo, R. F.; Chen, J. G. *J. Catal.* **2007**, *246*, 40−51.
(4) Molero, H.; Bartlett, B. F.; Tysoe, W. T. *J. Catal.* **1999**, *181*, 49−56.
(5) Weissermel, K.; Arpe, H. J. *Industrial ®ry*, 4th ed.; Wiley-VCH: Weinheim, Germany, 2003.
(6) Lee, J. M.; Palgunadi, J.; Kim, J. H.; Jung, S.; Choi, Y.-s.; Cheong, M.; Kim, H. S. *Phys. Chem. Chem. Phys.* **2010**, *12*, 1812−1816.
(7) Ramnial, T.; Ino, D. D.; Clyburne, J. A. C. *Chem. Commun.* **2005**, *3*, 325−327.
(8) Abbott, A. P.; Capper, G.; Davies, D. L.; Rasheed, R. H.; Tambyrajah, V. *Green Chem.* **2002**, *4*, 24−26.
(9) Bonhôte, P.; Dias, A. −P.; Papageorgiou, N.; Kalyanasundaram, K.; Grätzel, M. *Inorg. Chem.* **1996**, *35*, 1168−1178.
(10) Endres, F.; El Abedin, S. Z. *Phys. Chem. Chem. Phys.* **2006**, *8*, 2101−2116.
(11) Wishart, J. F.; Castner, E. W., Jr. *J. Phys. Chem. B* **2007**, *111*, 4639−4640.
(12) Rogers, R. D.; Voth, G. A. *Acc. Chem. Res.* **2007**, *40*, 1077−1078.
(13) Welton, T. *Chem. Rev.* **1999**, *99*, 2071−2084.
(14) Seddon, K. R. *J. Chem. Technol. Biotechnol.* **1997**, *68*, 351−356.
(15) Chiappe, C.; Pieraccini, D. *J. Phys. Org. Chem.* **2005**, *18*, 275−297.
(16) Ranke, J.; Stolte, S.; Störmann, R.; Arning, J.; Jastorff, B. *Chem. Rev.* **2007**, *107*, 2183−2206.
(17) Sun, H.; Qiao, B. F.; Zhang, D. J.; Liu, C. B. *J. Phys. Chem. A* **2010**, *114*, 3990−3996.
(18) Arce, A.; Earle, H.; Rodriguez, H.; Seddon, K. R.; Soto, A. *Green Chem.* **2008**, *10*, 1294−1300.
(19) Gao, H. S.; Li, Y. G.; Wu, Y.; Luo, M. F.; Li, Q.; Xing, J. M.; Liu, H. Z. *Energy Fuels* **2009**, *23*, 2690−2694.
(20) Scovazzo, P. *J. Membr. Sci.* **2009**, *343*, 199−211.
(21) Palgunadi, J.; Kang, J. E.; Nguyen, D. Q.; Kim, J. H; Min, B. K.; Lee, S. D.; Kim, H.; Kim, H. S. *Thermochim. Acta* **2009**, *494*, 94−98.
(22) Palgunadi, J.; Kim, H. S.; Lee, J. M.; Jung, S. *Chem. Eng. Process.* **2010**, *49*, 192−198.
(23) Jung, S.; Palgunadi, J.; Kim, J. H.; Lee, H.; Ahn, B. S.; Cheong, M.; Kim, H. S. *J. Membr. Sci.* **2010**, *354*, 63−67.
(24) Palgunadi, J.; Hong, S. Y.; Lee, J. K.; Lee, H.; Lee, S. D.; Cheong, M.; Kim, H. S. *J. Phys. Chem. B* **2011**, *115*, 1067−11074.
(25) Zhao, X.; Xing, H. B.; Yang, Q. W.; Li, R. L.; Su, B. G.; Bao, Z. B.; Yang, Y. W.; Ren, Q. L. *J. Phys. Chem. B* **2012**, *116*, 3944−3953.
(26) Frisch, M. J.; Trucks, G. W.; Schlegel, H. B.; Scuseria, G. E.; Robb, M. A.; Cheeseman, J. R.; Montgomery, J. A., Jr.; Vreven, T.; Kudin, K. N.; Burant, J. C.; Millam, J. M.; Iyengar, S. S.; Tomasi, J.; Barone, V.; Mennucci, B.; Cossi, M.; Scalmani, G.; Rega, N.; Petersson, G. A.; Nakatsuji, H.; Hada, M.; Ehara, M.; Toyota, K.; Fukuda, R.; Hasegawa, J.; Ishida, M.; Nakajima, T.; Honda, Y.; Kitao, O.; Nakai, H.; Klene, M.; Li, X.; Knox, J. E.; Hratchian, H. P.; Cross, J. B.; Bakken, V.; Adamo, C.; Jaramillo, J.; Gomperts, R.; Stratmann, R. E.; Yazyev, O.; Austin, A. J.; Cammi, R.; Pomelli, C.; Ochterski, J. W.; Ayala, P. Y.; Morokuma, K.; Voth, G. A.; Salvador, P.; Dannenberg, J. J.; Zakrzewski, V. G.; Dapprich, S.; Daniels, A. D.; Strain, M. C.; Farkas, O.; Malick, D. K.; Rabuck, A. D.; Raghavachari, K.; Foresman, J. B.; Ortiz, J. V.; Cui, Q.; Baboul, A. G.; Clifford, S.; Cioslowski, J.; Stefanov, B. B.; Liu, G.; Liashenko, A.; Piskorz, P.; Komaromi, I.; Martin, R. L.; Fox, D. J.; Keith, T.; Al-Laham, M. A.; Peng, C. Y.;

Nanayakkara, A.; Challacombe, M.; Gill, P. M. W.; Johnson, B.; Chen, W.; Wong, M. W.; Gonzalez, C.; Pople, J. A. *Gaussian 03*, Revision D.01; Gaussian, Inc.: Wallingford CT, 2004.
(27) Cornell, W. D.; Cieplak, P.; Bayly, C. I.; Gould, I. R.; Merz, K. M.; Ferguson, D. M.; Spellmeyer, D. C.; Fox, T.; Caldwell, J. W.; Kollman, P. A. *J. Am. Chem. Soc.* **1995**, *117*, 5179−5197.
(28) Liu, Z. P.; Huang, S. P.; Wang, W. C. *J. Phys. Chem. B* **2004**, *108*, 12978−12989.
(29) Wang, J. M.; Wolf, R. M.; Caldwell, J. W.; Kollman, P. A.; Case, D. A. *J. Comput. Chem.* **2004**, *25*, 1157−1174.
(30) Singh, U. C.; Kollman, P. A. *J. Comput. Chem.* **1984**, *5*, 129−145.
(31) Besler, B. H.; Merz, K. M.; Kollman, P. A. *J. Comput. Chem.* **1990**, *11*, 431−439.
(32) Bartlett, R. J.; Purvis, G. D. *Int. J. Quantum Chem.* **1978**, *14*, 561−581.
(33) Pople, J. A.; Binkley, J. S.; Seeger, R. *Int. J. Quantum Chem.* **1976**, *10*, 1−19.
(34) Liu, H. B.; Sale, K. L.; Holmes, B. M.; Simmons, B. A.; Singh, S. *J. Phys. Chem. B* **2010**, *114*, 4293−4301.
(35) Liu, H. J.; Maginn, E.; Visser, A. E.; Bridges, N. J.; Fox, E. B. *Ind. Eng. Chem. Res.* **2012**, *51*, 7242−7254.
(36) Berendsen, H. J. C.; van der Spoel, D.; van Drunen, R. *Comput. Phys. Commmun.* **1995**, *91*, 43−56.
(37) van der Spoel, D.; Lindahl, E.; Hess, B.; Groenhof, G.; Mark, A. E.; Berendsen, H. J. C. *J. Comput. Chem.* **2005**, *26*, 1701−1718.
(38) Hess, B.; Kutzner, C.; van der Spoel, D.; Lindahl, E. *J. Chem. Theory Comp.* **2008**, *4*, 435−447.
(39) Lindahl, E.; Hess, B.; van der Spoel, D. *J. Mol. Model.* **2001**, *8*, 306−317.
(40) Darden, T.; York, D.; Pedersen, L. *J. Chem. Phys.* **1993**, *98*, 10089−10092.
(41) Essmann, U.; Perera, L.; Berkowitz, M. L.; Darden, T.; Lee, H.; Pedersen, L. G. *J. Chem. Phys.* **1995**, *103*, 8577−8593.
(42) Berendsen, H. J. C.; Postma, J. P. M.; van Gunsteren, W. F.; DiNola, A.; Haak, J. R. *J. Chem. Phys.* **1984**, *81*, 3684−3690.
(43) Bondi, A. *J. Phys. Chem.* **1964**, *68*, 441−451.
(44) Shiflett, M. B.; Kasprzak, D. J.; Junk, C. P.; Yokozeki, A. *J. Chem. Thermodyn.* **2008**, *40*, 25−31.
(45) Morrow, T. I.; Maginn, E. J. *J. Phys. Chem. B* **2002**, *106*, 12807−12813.
(46) Yaws, C. L.; Miller, J. W.; Shah, P. N.; Schorr, G. R.; Patel, P. M. *Chem. Eng.* **1976**, *83*, 153−162.
(47) Keblinski, P.; Eggebrecht, J.; Wolf, D.; Phillpot, S. R. *J. Chem. Phys.* **2000**, *113*, 282−291.
(48) Bowron, D. T.; D'Agostino, C.; Gladden, L. F.; Hardacre, C.; Holbrey, J. D.; Lagunas, M. C.; McGregor, J.; Mantle, M. D.; Mullan, C. L.; Youngs, T. G. A. *J. Phys. Chem. B* **2010**, *114*, 7760−7768.
(49) Dupont, J. *J. Braz. Chem. Soc.* **2004**, *15*, 341−350.
(50) Jungwirth, P.; Tobias, D. J. *J. Phys. Chem. B* **2002**, *106*, 6361−6373.
(51) Gannon, T. J.; Law, G.; Watson, P. R. *Langmuir* **1999**, *15*, 8429−8434.
(52) Sloutskin, E.; Ocko, B. M.; Tamam, L.; Kuzmenko, I.; Gog, T.; Deutsch, M. *J. Am. Chem. Soc.* **2005**, *127*, 7796−7804.
(53) Sloutskin, E.; Ocko, B. M.; Tamam, L.; Kuzmenko, I.; Gog, T.; Deutsch, M. *J. Am. Chem. Soc.* **2005**, *127*, 18333−18333.
(54) Yan, T.; Li, S.; Jiang, W.; Gao, X.; Xiang, B.; Voth, G. A. *J. Phys. Chem. B* **2006**, *110*, 1800−1806.
(55) Bhargava, B. L.; Balasubramanian, S. *J. Am. Chem. Soc.* **2006**, *128*, 10073−10078.
(56) Pensado, A. S.; Malfreyt, P.; Pádua, A. A. H. *J. Phys. Chem. B* **2009**, *113*, 14708−14718.
(57) Perez-Blanco, M. E.; Maginn, E. J. *J. Phys. Chem. B* **2010**, *114*, 11827−11837.
(58) Wick, C. D.; Chang, T.-M.; Dang, L. X. *J. Phys. Chem. B* **2010**, *114*, 14965−14971.
(59) Lv, Y. Q.; Lin, Z. X.; Tan, T. W.; Feng, W.; Qin, P. Y.; Li, C. *Sens. Actuators, B* **2008**, *133*, 15−23.
(60) Zhang, H. Y.; Feng, W.; Li, C.; Tan, T. W. *J. Phys. Chem. B* **2010**, *114*, 4876−4883.